ACS APPLIED POLYMER MATERIALS

pubs.acs.org/acsapm

Article

# Vibronic States and Edge-On Oriented $\pi$-Stacking in Poly(3-alkylthiophene) Thin Films

Md Saifuddin, Saugata Roy, Subhankar Mandal, and Satyajit Hazra*

Cite This: *ACS Appl. Polym. Mater.* 2022, 4, 1377−1386

Read Online

ACCESS | Metrics & More | Article Recommendations | Supporting Information



**ABSTRACT:** The influence of alkyl side-chain length [$C_nH_{2n+1}$ (A), where $n$ = 6 (hexyl), 8 (octyl), 12 (dodecyl)] and thermal annealing (TA) and the definite roles of these in the quantity and quality of $\pi$-stacked crystallinity and edge-on orientated (EO) ordering of spin-coated poly(3-alkylthiophene) [P3AT] thin films, which are of massive significance in their optoelectronic properties, were investigated using complementary optical absorption spectroscopy and X-ray reflectivity (XR) techniques. The energy-band diagram, corresponding to the vibronic levels, obtained from the optical absorption spectrum provides information about the percentage, planarity, local order, and average conjugation length of the crystalline aggregates, while the electron density profile obtained from the XR provides unique information about the EO ordering and its variation along the depth. A prominent EO ordering near the substrate with a gradually decreased ordering toward the top surface is observed in each film. An as-cast P3HT film of shorter side-chain (having a natural nucleation tendency and rigidity) shows a slightly higher crystallinity and weaker excitonic coupling, while as-cast P3DDT film (having longer side-chain flexibility) shows a slightly better EO ordering. After the TA, the planarity of the unfolded backbone improves in each film; however, the effect is maximum in the P3DDT film. The EO ordering also improves throughout the film (by a thermal energy-induced reorientation of crystallites) but more toward the top surface (by increasing the decay length), preserving the exponential decay nature. The P3HT film (with the better initial crystallinity and planarity) shows an appreciable improvement, while the P3DDT film (where the crystallinity increases and crystallites have a better reorientational ability) shows the maximum improvement in the EO ordering. The improvement of the crystallinity (in quantity and quality) and the EO ordering of P3AT in thin films (as active layers), especially near the film−substrate interfaces, are of immense importance for their better in-plane charge carrier mobility in a thin-film transistor.

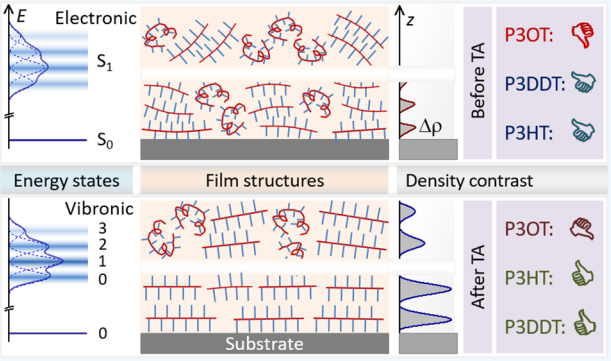


**KEYWORDS:** *conjugated polymers, optical absorption, X-ray reflectivity, vibronic levels, excitonic coupling, conjugation length, film−substrate interface, edge-on oriented ordering*

## 1. INTRODUCTION

The interest in organic semiconducting molecules and polymers have increased immensely in the last few decades due to their low cost and large-scale applications in printable electronics.[1−6] One important part of the printable transistors is the solution-processed semiconductor, which acts as an active layer in those devices.[7] Regioregular poly(3-alkylthiophene) (P3AT) comprises a significant and promising family of solution-processed conjugated polymers for use in printable electronics.[8,9] P3AT is composed of flexible alkyl side-chains attached to a stiff backbone consisting of thiophene units.[10] P3AT thin films contain crystalline domains along with some amorphous regions. Crystalline domains (or lamellar stacks) are formed due to strong $\pi-\pi$ interactions, perpendicular to the $\pi$-conjugation direction, between the thiophene rings of the neighboring polymer backbones and hydrophobic interactions between neighboring alkyl side-chains.[11] Crystalline domains can adopt two main orientations: edge-on and face-on, in which $\pi-\pi$ stackings are parallel and perpendicular to the substrate, respectively.[12] Charge transport within a crystalline domain is found better along the polymer backbone or intrachain $\pi$-conjugation direction (via charge delocalization), intermediate along the interchain $\pi$-stacking direction, and negligible along the insulating alkyl side-chain direction.[13,14] In a thin-film transistor (TFT),[15] where in-plane charge transport is important, edge-on oriented (EO) domains are preferred over face-on oriented domains, as in the former case the transport can be along $\pi$-conjugation as well as $\pi$-stacking directions (i.e., two-dimensional (2D)), while in the

Received: December 6, 2021
Accepted: January 20, 2022
Published: February 2, 2022

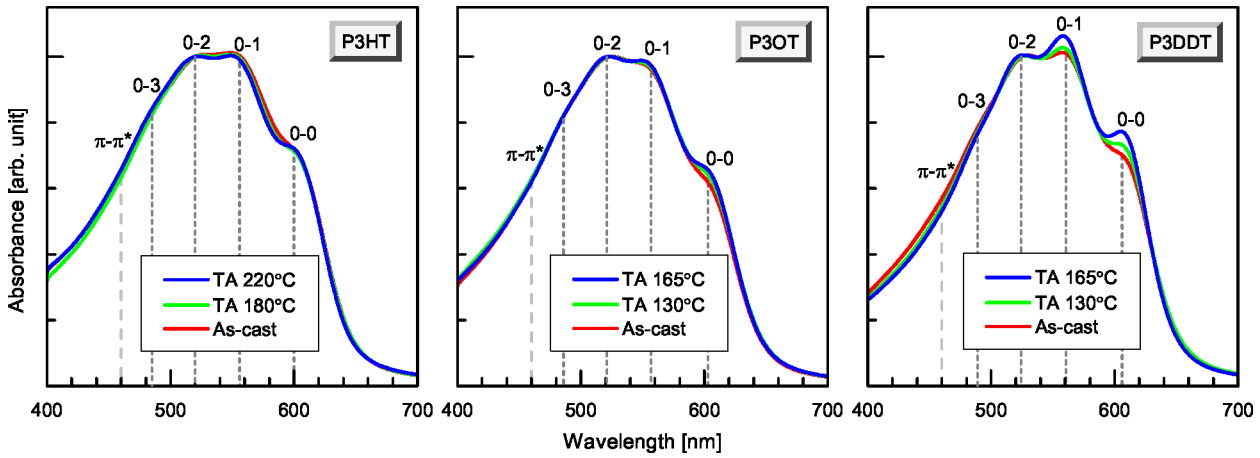


**Figure 1.** UV−Vis spectra (normalized by the 0−2 transition peak intensity) of the P3AT thin films of different alkyl chain length, before (as-cast) and after TA at different temperatures. The transition peaks, arising from amorphous ($\pi-\pi^*$) and weakly interacting H-aggregates, are indicated.

latter case it can be along a $\pi$-conjugation direction (i.e., one-dimensional (1D)) only.[16] However, the presence of domains, deviating from perfect EO crystallinity, along with the amorphous regions, in the thin film, usually creates a hindrance in the charge transport[17] and in its use in the actual market, despite its low manufacturing cost.[18] Thus, the improvement of the EO crystallinity, both in terms of quantity and quality, is important for obtaining better charge carrier mobility and device performances.

There are two aspects related to the improvement of EO crystallinity of P3HT active layers: one is the actual process of improvement itself, and another is the estimation or understanding such an improvement. Different processes or approaches have been exploited to improve the structure and to enhance the mobility.[18−22] It was evident that the structure of the P3AT thin film depends on many parameters such as regioregularity, molecular weight,[20] side-chain length,[22] casting solvent,[23] solvent aging,[24] substrate treatment,[25] deposition technique,[26] and postdeposition treatment.[27] An alkyl side-chain is one key parameter that determines the solubility of these polymers in organic solvents. The longer side-chains are better for the solubility, which facilitates the formation of smooth films for the fabrication of transistor devices by spin coating. However, the increasing chain length is supposed to reduce the field-effect mobility due to the insulating nature of the alkyl groups. Several groups have investigated the effect of side-chain length on the thin-film structure using different techniques and tried to correlate the structural changes with the charge carrier mobilities of P3AT thin films.[18,21] Despite a large number of works,[15] the effect of the alkyl side-chain on the thin-film structure, which in turn controls the mobility, is not completely understood. This is probably due to the lack of use of proper complementary techniques in understanding the quantity and quality of the overall and EO crystallinity in the film,[15,16,28,29] in general, and near the film−substrate interface,[30,31] in particular, which plays an important role in the charge transport, as the current in the bottom-gated TFT is known to move through the region of approximately the first few polymer layers at the film−substrate interface.[25]

The $\pi$-stacked P3ATs are inherently 2D excitonic systems with electronic excitations delocalized along the polymer chain as well as between chains.[32] Such excitons possess a dual nature; within polymer chains, excitons are of the Wannier-Mott type, where the electron and hole can readily separate over several repeat units, whereas across chains, excitons are more Frenkel-like, as charge separation is less likely and is limited to at most neighboring chains, resulting in the so-called interchain polarons.[32,33] On the one hand, the photophysical properties of such P3AT strongly depend on the quantity and quality of the crystalline aggregates, and thus the optical absorption can provide information about the aggregate percentage, the local aggregate order, and the conjugation length. On the other hand, the X-ray reflectivity (XR)[34,35] of a film strongly depends on its electron density profile (EDP), that is, the in-plane ($x-y$) average electron density ($\rho$) as a function of depth ($z$) in high resolution.[36,37] From the EDP it is possible to estimate the film thickness, the presence of layering in the film, if any, the structural arrangement near the film−substrate interface, and their evolution.[38−40] That means the XR can provide valuable information about the EO crystallites in the film, especially near the buried interface.

In this work, such complementary (optical absorption and XR) techniques were utilized to understand the effect of alkyl side-chain length [where alkyl (A) = hexyl (H), octyl (O), and dodecyl (DD)] and thermal annealing (TA) on the quantity and quality of the overall crystalline structures of spin-coated P3AT thin films, with an emphasis on the EO crystallites near the film−substrate interface, the improvement of which has immense importance in obtaining better charge transport properties. Indeed, a higher crystalline percentage and better crystalline quality are observed in the as-cast P3HT film compared to the as-cast P3OT and P3DDT films. Such a crystalline percentage and quality are found to evolve with TA in all the P3AT films. The structural evolution along the out-of-plane direction is quite significant for all the P3AT films, while that along the in-plane direction is found prominent for P3AT film with a longer side-chain. An attempt was made to understand the observed structural ordering and its evolution. Also, possible implications of such interesting structures on the charge carrier mobility are discussed.

## 2. EXPERIMENTAL DETAILS

P3HT (of average molecular weight (MW) 54 000−75 000 and regioregularity >98%), P3OT (of average MW 34 000 and regioregularity >98.5%), and P3DDT (of average MW 60 000 and regioregularity >98.5%) were purchased from Sigma-Aldrich and used as received. P3AT solutions of a similar concentration ($c$ = 4 mg/mL) were prepared by dissolving the polymer in a toluene solvent


https://doi.org/10.1021/acsapm.1c01772
ACS Appl. Polym. Mater. 2022, 4, 1377−1386

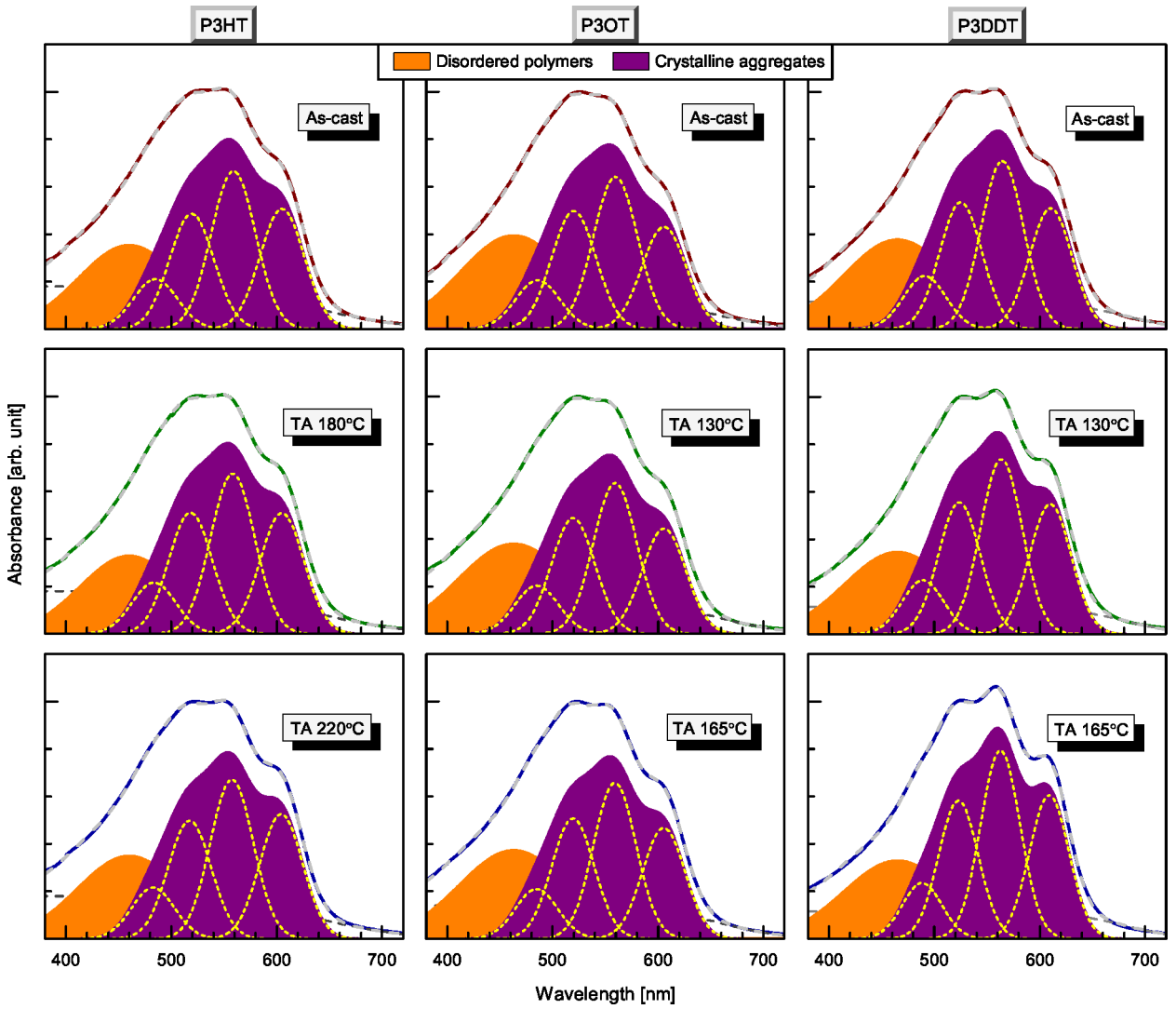


**Figure 2.** Measured (solid lines) and analyzed (dashed lines) optical absorption spectra (using eqs 1, 3, and 4) of the as-cast P3AT thin films of different alkyl side-chain length and after TA at different temperatures. Contributions of the disordered polymer chains and the crystalline aggregates are indicated by different filled colors. Deconvoluted transition peaks corresponding the crystalline aggregates are also indicated.

(obtained from Merck). The solutions were then sonicated for 5 min and annealed at 60 °C for 5 min to complete the dissolution. Before the film deposition, Si and quartz glass (QG) wafers (of size ~12 × 12 $mm^2$) were sonicated in acetone and ethanol to remove organic contaminates. P3AT films were then deposited on such QG and Si substrates by a spin-coating technique (using an SCS 6800 Spin Coater)[24] at a fixed spinning speed (1000 rpm) and time (60 s). Another set of films was also deposited on Si substrates at a higher spinning speed (2500 rpm). All films were subsequently heated at 70 °C for 15 min under a vacuum condition, and these are referred to as as-cast films. Films were also heated at different temperatures (from 130 to 220 °C as estimated from Figure S1 of the Supporting Information) for 20 min under a vacuum condition, and these are referred to as films after TA.

Optical (UV−vis) absorption spectra of the P3AT/QG thin films (before and after TA at different temperatures) were collected using a UV−vis spectrophotometer (JASCO, V-630).[24]

The XR measurements of the P3AT/Si thin films, in a wide dynamical range (~8 orders of magnitude), before and after TA at different temperatures, were performed using an X-ray diffractometer (Smartlab, Rigaku)[41,42] equipped with a copper source (sealed tube) followed by a Johansson Ge crystal and a parabolic multilayer mirror to obtain an intense parallel beam of Cu K$\alpha$1 radiation (of wavelength 1.54 Å). The scattered beam was detected using a point (NaI scintillation) detector. Data were taken in a specular condition; that is, the incident angle ($\theta$) is equal to the reflected angle ($\theta$), and both are in a scattering plane.[36,38,39] Under such a condition, there exists a nonvanishing wave-vector component $q_z$, which is given by $(4\pi/\lambda)\sin\theta$ with a resolution of 0.0014 $Å^{-1}$. The sample was placed horizontally and kept fixed on the goniometer base, whereas the source and the detector were rotated in a synchronized way.

## 3. RESULTS AND DISCUSSION

### 3.1. Optical Absorption and Crystalline Aggregates.

Optical absorption spectra (normalized with the peak intensity near 540 nm) of the P3HT, P3OT, and P3DDT thin films, before and after TA at different temperatures, which can provide useful information about the degree of intra- and interchain order within P3AT thin films,[32,43] are presented in Figure 1. Several peaks at higher wavelengths and a broad tail toward lower wavelengths are evident in the absorption spectra of all the films. The position, intensity, and/or shape of these films, however, vary a little bit with the alkyl chain length and TA. The intensity at a lower-wavelength tail and the positions of the higher-wavelength peaks are found to decrease and increase, respectively, with the increase of the alkyl chain



https://doi.org/10.1021/acsapm.1c01772
ACS Appl. Polym. Mater. 2022, 4, 1377−1386

length, while the peaks at higher wavelengths are found to become sharper with TA temperature. The peaks at higher wavelengths can be attributed to the transitions between states arising from aggregated or crystalline polymer,[44] whereas the broad tail near lower wavelength part can be attributed to the transitions between intraband states arising from the disordered polymer chains.[29] Accordingly, the optical absorption $I(\lambda)$ can be considered as a combination of two parts

$$I(\lambda) = I_c(\lambda) + I_a(\lambda) \quad (1)$$

where $I_c(\lambda)$ is the contribution due to the crystalline ($\pi$-stacking of rod-like) polymers, and $I_a(\lambda)$ is the contribution due to the amorphous or disordered (coil-like) polymers.

The crystalline polymers can be considered as weakly interacting H-aggregates, in which the excitonic motions are only along the interchain $\pi-\pi$ stacking direction.[45,46] Then the crystalline contribution in the absorption can be expressed using a series of Gaussian peaks (similar to the Frank−Condon progression) associated with the transitions between states arising from such weakly interacting H-aggregates as[24,47]

$$I_c(\lambda) = \sum_j I_{0-j}\exp[-\{(\lambda - \lambda_{0-j})/\sigma_j\}^2] \quad (2)$$

where $I_{0-j}$ is the intensity, $\lambda_{0-j}$ is the position, and $\sigma_j$ is the width of the $0-j$ transition-related Gaussian peak. Considering peaks are equally spaced (in the energy scale by $E_p$) and have the same width ($\sigma_c$), eq 2 can be written as

$$I_c(\lambda) = \sum_j I_{0-j}\exp\left[-\left\{\left(\lambda - \frac{hc\lambda_{0-0}}{hc + jE_p\lambda_{0-0}}\right)/\sigma_c\right\}^2\right] \quad (3)$$

where $h$ is the Planck's constant, $c$ is the velocity of light, and $hc$ = 1239.8 eV nm.

Similarly, the amorphous part can be expressed using a broad Gaussian peak, associated with the intrachain $\pi-\pi^*$ transition (unlike considering it as the difference between the experimental absorption and the modeled aggregate component[16,48]) as

$$I_a(\lambda) = I_{a,0}\exp[-\{(\lambda - \lambda_a)/\sigma_a\}^2] \quad (4)$$

where $I_{a,0}$ is the intensity, $\lambda_a$ is the position, and $\sigma_a$ is the width of the Gaussian peak. Then the relative amounts of the crystalline and amorphous parts ($A_c$ and $A_a$) in the film can be estimated considering the area under the curves as

$$A_c = \sqrt{\pi}\sigma_c \sum_j I_{0-j} \quad (5)$$

$$A_a = \sqrt{\pi}\sigma_a I_{a,0} \quad (6)$$

Further, owing to the interband mixing in the weakly interacting H-aggregates, the intensity ratio of the 0−0 and 0−1 vibronic lines ($I_{0-0}/I_{0-1}$) is related to the nearest-neighbor interchain Coulombic coupling ($J_0 > 0$) via the free-exciton bandwidth ($W = 4J_0$) of the aggregates and the energy of the main intramolecular vibration ($E_p$) coupled to the electronic transition.[32] Assuming the Huang−Rhys factor to be unity, $W$ can be expressed as[45,46]

$$W \approx E_p\frac{1 - \sqrt{I_{0-0}/I_{0-1}}}{0.24 + 0.073\sqrt{I_{0-0}/I_{0-1}}} \quad (7)$$

where an increase in the $I_{0-0}/I_{0-1}$ ratio corresponds to a decrease in the $W$ value and the excitonic coupling and, therefore, an increase in the conjugation length (or planarity) and the degree of intrachain order.[49,50]

The optical absorption spectra, simulated using eqs 1, 3, and 4, are shown in Figure 2. For the simulation, four peaks (i.e., $j$ = 4) for the crystalline part and a background in the form of an error function were considered. The relevant parameters, namely, $\lambda_{0-0}$, $\sigma_c$, $E_p$, and $I_{0-0}/I_{0-1}$, as obtained from the analysis, are shown in Table 1. Also, the fraction of crystalline aggregates [$f_c = A_c/(A_a + A_c)$], obtained using eqs 6 and 5, and the values of $W$, estimated using eq 7, are listed in Table 1.

**Table 1. Parameters**[a]

| sample | treatment | $f_c$ | $\lambda_{0-0}$ [nm] | $\sigma_c$ [nm] | $E_p$ [meV] | $I_{0-0}/I_{0-1}$ | $W$ [meV] |
|---|---|---|---|---|---|---|---|
| P3HT | as-cast | 0.70 | 605.1 | 29.8 | 169 | 0.76 | 71 |
| | TA 180 °C | 0.72 | 605.0 | 29.4 | 172 | 0.76 | 74 |
| | TA 220 °C | 0.69 | 604.3 | 28.8 | 172 | 0.78 | 65 |
| P3OT | as-cast | 0.65 | 605.7 | 29.8 | 169 | 0.67 | 101 |
| | TA 130 °C | 0.65 | 605.7 | 29.2 | 170 | 0.70 | 92 |
| | TA 165 °C | 0.66 | 605.4 | 28.4 | 170 | 0.71 | 88 |
| P3DDT | as-cast | 0.68 | 610.4 | 28.5 | 165 | 0.72 | 83 |
| | TA 130 °C | 0.70 | 610.0 | 27.9 | 167 | 0.74 | 76 |
| | TA 165 °C | 0.71 | 609.0 | 26.6 | 168 | 0.76 | 70 |

[a]Parameters, such as the fraction of crystalline aggregates ($f_c$), the position of 0−0 transitional peak ($\lambda_{0-0}$), the width of the Gaussian transitional peaks ($\sigma_c$), the intramolecular vibrational energy ($E_p$), the intensity ratio ($I_{0-0}/I_{0-1}$), and the exciton bandwidth ($W$) for the P3AT thin films of different alkyl side-chain length after different treatments as obtained from the analysis of the absorption spectra.

Small changes in the values of different parameters with alkyl chain length and TA temperature are evident in Table 1. In the as-cast condition, the value of $f_c$ is maximum for the P3HT film and minimum for the P3OT film, while the value of $W$ is the reverse. This indicates that the crystallinity and conjugation length are best in the as-cast P3HT film and worst in the as-cast P3OT film, which is likely to be related to their nucleation tendency in solution. A better or faster nucleation tendency is expected for the P3HT, where the growth of nanofibers/aggregates due to solution aging have been observed before,[24] while the present result suggests the least nucleation tendency for the P3OT. The lowest $W$ value in the as-cast P3HT thin film, compared to the as-cast P3OT and P3DDT thin films, indicates a more planar backbone structure inside the aggregate probably due to the diminished flexibility of the shorter alkyl chains. Also, a small increase in the value of $\lambda_{0-0}$ but a small decrease in the values of $\sigma_c$ and $E_p$ with the increase in the alkyl chain length is observed. These probably indicate a slight decrease in the band gap, a slight increase in the local aggregate ordering, and a slight damping in the intramolecular vibration with the increase in alkyl chain length.

However, a small increase (or decrease) in the value of $f_c$ (or $W$) with the increase in the annealing temperature is observed for all the films except for the P3HT film, where $f_c$ (or $W$) is found as the maximum (or minimum) at 180 °C (or 220 °C). A small increase (or decrease) in the value of $f_c$ (or $W$) with



https://doi.org/10.1021/acsapm.1c01772
ACS Appl. Polym. Mater. 2022, 4, 1377−1386

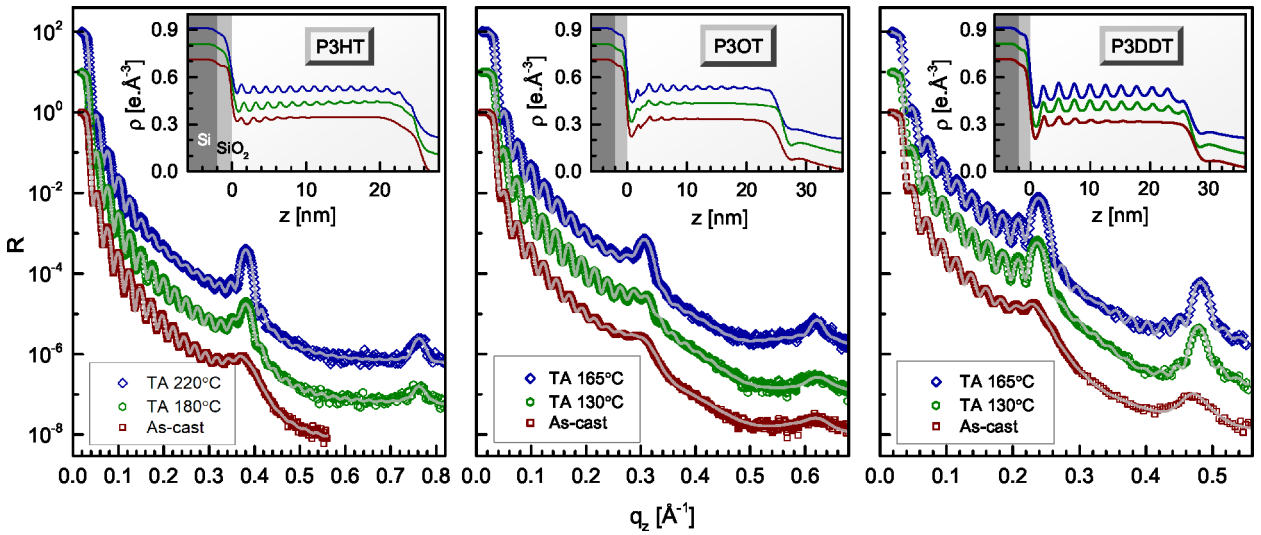


**Figure 3.** Evolution of XR profiles (different symbols) and analyzed curves (solid lines) of the P3AT thin films of different alkyl chain length during TA at different temperatures. (inset) Corresponding analyzed EDPs. Curves and profiles are shifted vertically for clarity.

**Table 2. Parameters**[a]

| sample | treatment | $D$ [nm] | $\rho_a$ [e Å$^{-3}$] | $N$ | $d$ [nm] | $\Delta\rho_a$ [e Å$^{-3}$] | $\Delta\rho'_m$ [e Å$^{-3}$] | $\Delta\rho_m$ [e Å$^{-3}$] | $\zeta$ [nm] |
|---|---|---|---|---|---|---|---|---|---|
| P3HT | as-cast | 25.8 | 0.35 | 15 | 1.67 | 0.01 | 0.03 | 0.03 | 4 |
| | TA 180 °C | 25.3 | 0.35 | 15 | 1.65 | 0.02 | 0.06 | 0.05 | 9 |
| | TA 220 °C | 25.3 | 0.35 | 15 | 1.65 | 0.03 | 0.06 | 0.04 | 30 |
| P3OT | as-cast | 25.9 | 0.34 | 12 | 2.05 | 0.01 | 0.03 | 0.03 | 3 |
| | TA 130 °C | 26.0 | 0.34 | 12 | 2.01 | 0.01 | 0.03 | 0.03 | 4 |
| | TA 165 °C | 25.7 | 0.34 | 12 | 2.03 | 0.03 | 0.05 | 0.05 | 11 |
| P3DDT | as-cast | 27.7 | 0.32 | 10 | 2.67 | 0.03 | 0.08 | 0.05 | 5 |
| | TA 130 °C | 27.3 | 0.32 | 10 | 2.63 | 0.07 | 0.09 | 0.08 | 21 |
| | TA 165 °C | 27.3 | 0.32 | 10 | 2.61 | 0.08 | 0.10 | 0.10 | 25 |

[a]Parameters, such as the average thickness ($D$), the average electron density ($\rho_a$), the number of bilayer repetition ($N$), the average electron density contrast ($\Delta\rho_a$), the maximum electron density contrast at the interfacial bilayer ($\Delta\rho'_m$) and second bilayer ($\Delta\rho_m$), and the critical decay length ($\zeta$) of the as-cast and TA P3AT thin films, as obtained from the XR data analysis.

the increase in the annealing temperature suggests an improvement of the crystallinity and planarity/conjugation length in the film with TA. The thermal energy probably promotes the unfavorable coil-to-rod conformational transformation of some of the P3AT polymer chains and their unfavorable $\pi-\pi$ stacking and hence in the increase of crystalline aggregates. The overall crystallinity with TA mainly increases with longer side-chains, because longer side-chains are more flexible and mobile, which may cause faster/better crystallization.[51] Also, with the increase in the annealing temperature the values of $\lambda_{0-0}$ and $\sigma_c$ either remain the same or decrease a little bit, while the value of $E_p$ either remains the same or increases a little bit. These probably indicate a slight increase in the band gap (probably due to a decrease in the band dispersion), a slight increase in the local aggregate ordering, and a slight reduction in the damping of the intramolecular vibration (i.e., more relaxed, probably due to the improvement in the planarity) with thermal annealing.

**3.2. EDP and EO Crystalline Aggregates.** XR profiles, which can provide useful structural information on the films along the $z$-direction, are shown in Figure 3, for the as-cast and annealed (at different temperatures) P3HT, P3OT, and P3DDT thin films. The Kiessig fringes, which are the measure of the total film thickness ($D$), are evident in all the XR profiles.[52] The estimated $D$ values (~25−27 nm) are the commonly used thickness for organic TFT devices.[22] Sharp peaks at $q_z \approx 0.38$ and 0.76 Å$^{-1}$ for the P3HT film, at $q_z \approx 0.31$ and 0.62 Å$^{-1}$ for the P3OT film, and at $q_z \approx 0.24$ and 0.48 Å$^{-1}$ for the P3DDT film are also evident in the XR profiles, which correspond to the first- and second-order pseudo-Bragg peaks of the EO ordering. The positions of such peaks provide the bilayer thickness ($d$), while the width of the peak provides the crystallite size or correlation length ($\xi$) of the EO-ordered structures along the $z$-direction. The $d$ values estimated for P3HT, P3OT, and P3DDT films are 1.64, 2.0, and 2.63 nm, respectively. The positions of Kiessig fringes and pseudo-Bragg peaks remain almost unchanged after TA suggesting no appreciable change in the $D$ and $d$ values, while the intensity (width) of a pseudo-Bragg peak increases (decreases) with TA suggesting an increase in the amount (extent) of EO ordering in the films. The evolution of EO ordering with TA is also evident from the typical X-ray diffraction (XRD) maps across the first Bragg peak for the P3HT film (shown in Figure S2 of the Supporting Information).

To get more quantitative information about the structure of the film, especially about the EO ordering, the XR data were analyzed using a matrix method after the roughness was incorporated at each interface.[53,54] An instrumental resolution



https://doi.org/10.1021/acsapm.1c01772
ACS Appl. Polym. Mater. 2022, 4, 1377−1386

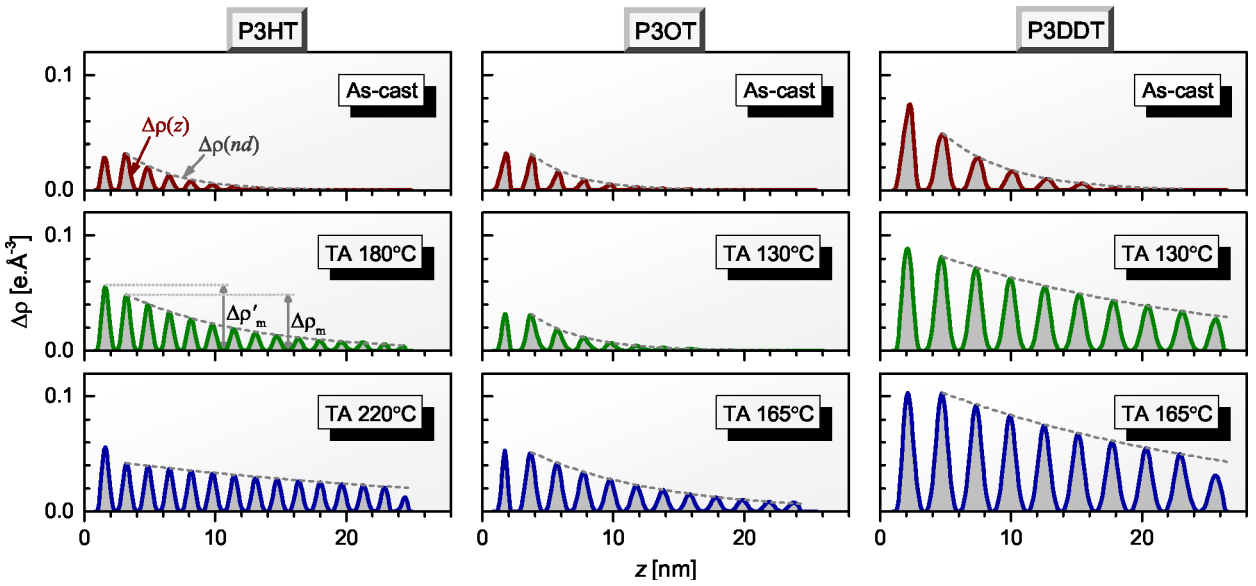


**Figure 4.** Variation of electron density contrast ($\Delta\rho$) as a function of height ($z$) and in bilayer steps ($nd$) for the P3AT thin films of different alkyl chain length before (as-cast) and after TA at different temperatures. $\Delta\rho'_m$ and $\Delta\rho_m$, which represent the maximum electron density contrast for the first (or interfacial) bilayer and second bilayer (actually used in eq 8), respectively, are indicated.

in the form of a Gaussian function and a constant background were also included at the time of data analysis.[40] For the analysis, first each film was considered as a single layer after incorporating an interfacial oxide layer ($SiO_2$) above the substrate (Si). The simulation based on such model, though not up to the mark (shown in the left-hand side of Figures S3−S5 of the Supporting Information), can provide the average thickness ($D$) and the average electron density ($\rho_a$) of the film as shown in Table 2. Next each film of thickness $D$ was divided into a number of bilayers after an interfacial oxide layer was incorporated above the substrate.[12,24,55] Each bilayer of thickness $d$ consists of a high electron density ($\rho_{bb}$) polythiophene backbone layer of thickness $d_{bb}$ and a low electron density ($\rho_{sc}$) alkyl side-chain containing a layer of thickness $d_{sc}$. A simulation was then performed considering the bilayer ($d = d_{bb} + d_{sc}$) stack of uniform electron density contrast ($\Delta\rho = \rho_{bb} - \rho_{sc}$) along the $z$-direction. The simulated XR profile and the corresponding EDP thus obtained (shown in the right-hand side of Figures S3−S5 of the Supporting Information) provide the bilayer repetition ($N$), bilayer thickness ($d$), and bilayer electron density contrast ($\Delta\rho_a$) of the film as shown in Table 2. Though such a simulation reproduced the positions, it was unable to reproduce all the features (mainly intensities) of the XR data properly.

To overcome this problem, further variation of $\Delta\rho$ along the $z$-direction was necessary.[24] Owing to the fact that the slow evaporation of solvent near the film−substrate interface (i.e., larger time) is likely to help the organization of the polymers and their ordering there, while the fast evaporation of a solvent near a film−air interface (i.e., less time) is likely to restrict the organization of the polymers and their ordering at top, the variation of $\Delta\rho$ as a function of height can be expressed as

$$\Delta\rho(nd) = \Delta\rho_m \exp(-nd/\zeta) \tag{8}$$

where $n$ is an integer, $\Delta\rho_m$ is the maximum electron density contrast, and $\zeta$ is the critical decay length. The large $\Delta\rho_m$ value is related to the better in-plane ordering toward film−substrate interface, and a large $\zeta$-value suggests a better extent of ordering along the out-of-plane direction, which is related to the improvement of the in-plane ordering more toward the film−air interface. $\zeta \to \infty$ indicates $\Delta\rho(nd) = \Delta\rho_m$, that is, uniform density contrast throughout the $z$-direction. Using eq 8, the variations of $\rho_{bb}$ (peak) and $\rho_{sc}$ (dip) with height can be expressed as

$$\rho_{bb}(nd) = \rho_a + (d_{sc}/d)\Delta\rho_m \exp(-nd/\zeta) \tag{9}$$

$$\rho_{sc}(n'd) = \rho_a - (d_{bb}/d)\Delta\rho_m \exp(-n'd/\zeta) \tag{10}$$

where $n' = n + 1/2$. Here, $d_{sc}/d$ and $d_{bb}/d$ (where $d_{sc}/d_{bb} > 1$) terms are used to incorporate a greater deviation in $\rho_{bb}$ compared to $\rho_{sc}$ (with respect to (wrt) the average value $\rho_a$). A separate interfacial bilayer was also considered to take care of the effect of the substrate surface energy on the growth of the film. The maximum electron density contrast of that interfacial (i.e., first) bilayer is represented by $\Delta\rho'_m$. Subsequently, eqs 8−10 are used for the second bilayer onward, where $n = 0$ and $\Delta\rho_m$ essentially represent the position and maximum contrast, respectively, of the second bilayer. The best-fit XR profiles along with the corresponding EDPs thus obtained for different films are presented in Figure 3. The corresponding electron density contrast ($\Delta\rho$) as a function of height ($z$), which is of prime interest for understanding the EO ordering of the films, is plotted in Figure 4. The relevant parameters such as $\Delta\rho'_m$, $\Delta\rho_m$, and $\zeta$ for the as-cast and TA P3AT thin films are then listed in Table 2.

The values of $\Delta\rho'_m$, $\Delta\rho_m$, and $\zeta$ for the as-cast P3DDT film are found to be higher compared to other as-cast P3AT films. The flexibility of the longer alkyl chain probably helps the improvement in the initial organization and EO ordering of the as-cast P3DDT film over other films. The values of $\Delta\rho'_m$, $\Delta\rho_m$, and $\zeta$ for all the films are found to increase after TA. The increasing pattern, however, varies slightly with alkyl chain length. In the case of a P3HT film, the $\Delta\rho'_m$ value first increases slightly and then remains the same, while the $\Delta\rho_m$ value first increases (slightly) and then decreases (slightly), and the $\zeta$-value increases gradually with the annealing temperature. This indicates a low-temperature (180 °C) annealing improved the


https://doi.org/10.1021/acsapm.1c01772
ACS Appl. Polym. Mater. 2022, 4, 1377−1386

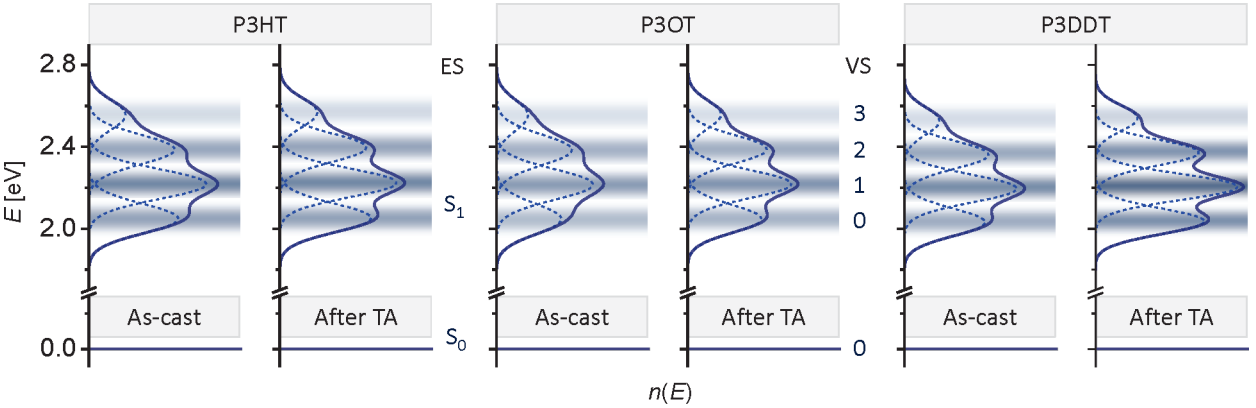


**Figure 5.** Energy-band diagrams (corresponding to the crystalline part) of the P3AT thin films of different alkyl side-chain length before (as-cast) and after TA as obtained from the optical absorption spectra showing vibronic levels/states (VS) corresponding to the ground ($S_0$ or HOMO) and first exited ($S_1$ or LUMO) electronic levels/states (ES) arising from exciton−phonon coupling in the weakly interacting H-aggregates.

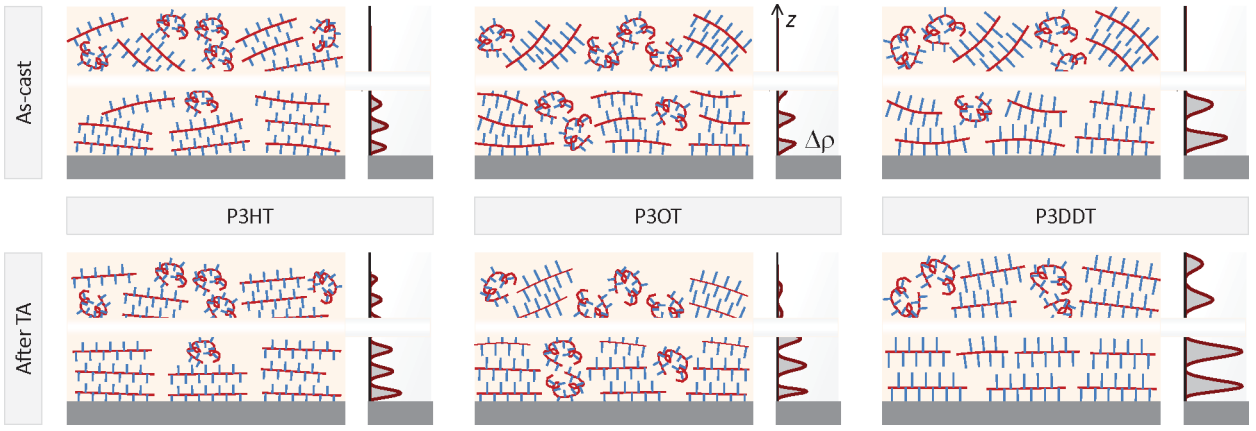


**Figure 6.** Structural schematics, along with the electron density contrast ($\Delta\rho$), of the P3AT thin films of different alkyl side-chain lengths before (as-cast) and after TA as obtained from the optical absorption and XR data analysis showing amorphous (coil-like) and crystalline aggregated (due to $\pi$-conjugation of rod-like) polymers of different fraction, backbone length, planarity, and orientation, both near and away from the substrate.

EO ordering throughout the film, while the high-temperature (220 °C) annealing only improved the EO ordering toward the top surface of the film. In the case of P3OT film, there was almost no change in the values of $\Delta\rho'_m$, $\Delta\rho_m$, and $\zeta$ (hence the EO ordering) after a low-temperature (130 °C) annealing, while a slight increase occurred in the values of all the parameters (hence the EO ordering) after a high-temperature (165 °C) annealing. Finally, in the case of P3DDT film, an appreciable increase in the values of $\Delta\rho'_m$, $\Delta\rho_m$, and $\zeta$ (hence the EO ordering) were observed even after a low-temperature (130 °C) annealing and a further increase after a high-temperature (165 °C) annealing. It can be noted that the information on EO ordering for the high-thickness films prepared at 1000 rpm is also consistent with that obtained for the low-thickness films prepared at 2500 rpm (shown in Figure S6 of the Supporting Information). The thermal energy-induced reorientation (major) and growth (minor) of crystalline domains, which are mainly responsible for the increase in the EO ordering in the film, not only depends on the thermal energy (temperature) itself but also on the flexibility and mobility (alkyl chain) of the polymer.

**3.3. Overall Structures and Their Implications.** Let us first represent the energy-band (EB) diagrams of the crystalline part of the P3AT films and then the overall structures of the films and their possible implications in the device properties. The EB diagrams, as obtained from the analysis of the optical absorption spectra, are presented in Figure 5. The energy of the vibronic levels of the first exited electronic state ($S_1$, also known as lowest unoccupied molecular orbital or LUMO) are presented with respect to the zeroth vibronic level of the ground electronic state ($S_0$, also known as highest occupied molecular orbital or HOMO). The energy of the zeroth vibronic level is obtained from the $\lambda_{0-0}$ value, which is related to the HOMO−LUMO gap plus the exciton binding energy. The contribution of the latter can be neglected in the first approximation. The separation and width of the vibronic levels are obtained from the $E_p$ and $\sigma_c$ values, respectively, while the contrast of the $j$th vibronic level is obtained from the $I_{0-j}$ value, which can be correlated with the density of state (DOS) in the first approximation (by neglecting the effect of the oscillator strength in the transition). The overall increase of such a DOS indicates an increase in the crystalline aggregates in the film, while the increase in the DOS of the zeroth vibronic level, relative to the first vibronic level, indicates a weakening of the excitonic coupling and an improvement of the conjugation length.

The structures of the P3AT films can be modeled by combining the complementary information obtained from the optical absorption (or EB diagrams) and the XR (or $\Delta\rho$ profiles) as shown schematically in Figure 6. In the as-cast condition, the crystallinity ($f_c$) is found as a maximum in the P3HT film and as a minimum in the P3OT film. P3ATs with


https://doi.org/10.1021/acsapm.1c01772
ACS Appl. Polym. Mater. 2022, 4, 1377−1386

shorter side-chains are known to show the solution aging effect,[24,56] which indicates their natural nucleation tendency. Such a nucleation tendency seems to enhance the crystallinity of the as-cast P3HT film over other films. In the case of P3DDT, the longer side-chain makes the backbone flexible, which helps the ordering and the crystallinity, to some extent. On the one hand, P3OT of an intermediate chain length neither has the natural nucleation tendency nor has that flexibility, resulting in a minimum crystallinity. On the other hand, the rigidity of the P3HT (having a shorter side-chain) seems to enhance the planarity of its unfolded backbone and hence the conjugation length (i.e., relatively weaken the excitonic coupling), while the flexibility of the P3DDT (having a longer side-chain) seems to enhance the length of its unfolded backbone and hence the conjugation length to some extent. The intermediate chain length of P3OT lacks the enhancements of both planarity and length of the unfolded backbone and hence the conjugation length (i.e., it relatively strengthens the excitonic coupling). In the as-cast films, the EO ordering is found as prominent near the film−substrate interface and gradually less prominent (following an exponential decay nature) with height due to the relatively high reorganization time arising from a relatively slow solvent evaporation at that film−substrate interface and a gradually slow reorganization time toward the top surface during a deposition. It is known that the high regioregularity of P3AT has a massive effect in the chain packing as well as in the EO ordering.[13] Such EO ordering is found as a maximum in the P3DDT film due to its low viscosity (arising from flexibility) and as a minimum in the P3OT film due to the lack of its flexibility and crystallinity, while the intermediate in the P3HT film is due to its better crystallinity (arising from natural nucleation tendency).

In general, the crystallinity, conjugation length (i.e., planarity and/or length of the unfolded backbone), and EO ordering of the P3AT films are expected to increase after TA (due to the thermal energy), especially near the melting temperature of the polymer backbones ($T_2$ was estimated from Figure S1 of the Supporting Information). In particular, the crystallinity ($f_c$) is found to increase in the P3DDT film only, which indicates that the flexibility of the longer side-chain, in the presence of thermal energy, essentially enhances the backbone mobility and the crystallinity. The planarity of the unfolded backbone seems to increase (i.e., the excitonic coupling relatively weaken) with the thermal energy (due to relaxation) for all the films; however, the effect is maximum for the P3DDT film, where the unfolded backbone length is maximum. In the case of P3OT film, where the unfolded backbone length is minimum, the effect is also a minimum. The major effect of the thermal energy is, however, on the EO ordering of the P3AT. The thermal energy mainly helps in the reorientation of the crystalline aggregates, rather than their growth, to attend the EO ordering (which is probably favorable or an energy-minimum configuration[55,57]). The EO ordering is found to improve gradually throughout the film with the increase of thermal energy (i.e., annealing temperature). Though the exponential decay nature with the film height is still maintained even after TA, the decay length increases appreciably; that is, the difference between the EO ordering toward film−substrate and film−air interfaces decreases. However, the EO ordering improvement is maximum in the P3DDT film, which is probably related to the slight improvement in the crystallinity and their better reorientational ability (arising from a longer side-chain flexibility). The improvement of EO ordering in the P3HT film is also appreciable, which can be correlated with the better initial crystallinity and planarity. The improvement of EO ordering is minimum in the P3OT film, which is probably due to their diminished flexibility (or reorientational ability) and lack of improvement in the crystallinity.

The better crystalline quantity (or overall DOS) and quality (i.e., relatively weaker excitonic coupling) of the aggregates in the as-cast P3HT thin film is likely to provide better charge carrier mobility compared to the as-cast P3OT and P3DDT thin films as reported before,[18] while better EO ordering near the film−substrate interface in the as-cast P3DDT thin film, unlike what has been reported before,[18] is likely to provide better in-plane charge carrier mobility over others. On the one hand, considering all parameters, the P3HT thin film is expected to provide the best performance in the as-cast condition consistent with earlier reported observations. On the other hand, the device performance of all films after TA is expected to improve much due to the improvement in most of the parameters.[21] However, the charge carrier mobility or device performance is expected to be a maximum in the P3DDT film, where the crystalline quantity (overall DOS), the local aggregate order (obtained from bandwidth), and EO ordering, both near the film−substrate interface and away from it, improve appreciably after TA. Also, an almost comparable device performance is expected for the P3HT film, where the least excitonic coupling (i.e., best crystalline quality) and a better overall EO ordering are observed after TA. It can be noted that the implication of the structure on the device performance has been predicted considering the quality, quantity, and orientation of the crystalline aggregates and not considering the quality of the connection between aggregates. The latter is also likely to play an important role in the governance of the overall charge transport in the system, and any major changes in it can create an appreciable change in the overall performance.

## 4. CONCLUSIONS

Optical absorption (UV−vis) spectroscopy and XR techniques were utilized to understand the effect of alkyl side-chain length and thermal annealing on the growth and evolution of the P3AT thin films. In particular, the EB diagram obtained from the optical absorption spectrum provides information about the quality (planarity, local order, and average conjugation length) and quantity (fraction) of the crystalline aggregates, while the EDP obtained from the XR profile provides information about their orientation (namely, EO), especially near the film−substrate interface. The better crystalline percentage and relatively weaker excitonic coupling of the crystalline aggregates (related to their nucleation tendency and rigidity arising from the shorter side-chain) are observed in the as-cast P3HT thin film, while a better EO ordering near the film−substrate interface (related to its longer side-chain flexibility) is observed in the as-cast P3DDT thin film. After TA, the crystallinity is found to increase (due to the enhanced backbone mobility of the flexibility of a longer side-chain) in the P3DDT film only. The planarity of the unfolded backbone is found to increase with the thermal energy for each film; however, the effect is a maximum for the P3DDT film, where the unfolded backbone length is a maximum. The EO ordering is found to improve gradually throughout the film mainly due to the thermal energy-induced reorientation of crystallites. The improvement is a maximum in the P3DDT film, which is


https://doi.org/10.1021/acsapm.1c01772
ACS Appl. Polym. Mater. 2022, 4, 1377−1386

related to a small improvement in the crystallinity and the better reorientational ability of the film. The improvement of EO ordering in the P3HT film is also appreciable, which is related with the better initial crystallinity and planarity. Such complementary but distinctive information on the P3AT thin films is very important and useful for the improvement of TFT properties.

## ■ ASSOCIATED CONTENT

### Supporting Information

The Supporting Information is available free of charge at https://pubs.acs.org/doi/10.1021/acsapm.1c01772.

Estimation of melting temperatures of P3AT powders from DSC thermograms; XRD maps for P3HT film; estimation of relevant parameters through XR data simulation (PDF)

## ■ AUTHOR INFORMATION


### Corresponding Author

**Satyajit Hazra** − *Saha Institute of Nuclear Physics, A CI of Homi Bhabha National Institute, Kolkata 700064, India;* orcid.org/0000-0001-5592-2078; Email: satyajit.hazra@saha.ac.in

### Authors

**Md Saifuddin** − *Saha Institute of Nuclear Physics, A CI of Homi Bhabha National Institute, Kolkata 700064, India;* orcid.org/0000-0003-1416-3081

**Saugata Roy** − *Saha Institute of Nuclear Physics, A CI of Homi Bhabha National Institute, Kolkata 700064, India*

**Subhankar Mandal** − *Saha Institute of Nuclear Physics, A CI of Homi Bhabha National Institute, Kolkata 700064, India*

Complete contact information is available at: https://pubs.acs.org/10.1021/acsapm.1c01772


### Notes

The authors declare no competing financial interest.

## ■ ACKNOWLEDGMENTS

The authors thank Mr. G. Sarkar, Dr. R. Dev Das, and Ms. S. Roy for their help in the thin-film preparation, XR, and UV−vis measurements, respectively. The authors also thank Prof. M. Mukhopadhyay for providing the X-ray facility. M.S. acknowledges University Grant Commission (UGC), India, and S.M. acknowledges Council of Scientific & Industrial Research (CSIR), India, for providing research fellowships.

## ■ REFERENCES


(1) Yu, G.; Gao, J.; Hummelen, J. C.; Wudl, F.; Heeger, A. J. Polymer Photovoltaic Cells: Enhanced Efficiencies via a Network of Internal Donor−Acceptor Heterojunctions. *Science* **1995**, *270*, 1789−1791.

(2) Yan, H.; Chen, Z.; Zheng, Y.; Newman, C.; Quinn, J. R.; Dötz, F.; Kastler, M.; Facchetti, A. A High-Mobility Electron-Transporting Polymer for Printed Transistors. *Nature* **2009**, *457*, 679−686.

(3) Facchetti, A. π-Conjugated Polymers for Organic Electronics and Photovoltaic Cell Applications. *Chem. Mater.* **2011**, *23*, 733−758.

(4) Wang, T.; Pearson, A. J.; Lidzey, D. G. Correlating Molecular Morphology with Optoelectronic Function in Solar Cells Based on Low Band-gap Copolymer: Fullerene Blends. *J. Mater. Chem. C* **2013**, *1*, 7266−7293.

(5) Reynolds, J. R.; Thompson, B. C.; Skotheim, T. A. *Conjugated Polymers: Properties, Processing, and Applications;* CRC Press: Boca Raton, FL, 2019.

(6) Mandal, S.; Mukherjee, M.; Hazra, S. Evolution of Electronic Structures of Polar Phthalocyanine−Substrate Interfaces. *ACS Appl. Mater. Interfaces* **2020**, *12*, 45564−45573.

(7) Diao, Y.; Shaw, L.; Bao, Z.; Mannsfeld, S. C. B. Morphology Control Strategies for Solution-Processed Organic Semiconductor Thin Films. *Energy Environ. Sci.* **2014**, *7*, 2145−2159.

(8) Dierckx, W.; Oosterbaan, W. D.; Bolsée, J.-C.; Maes, W.; Vanderzande, D.; Manca, J. Poly(3-alkylthiophene) Nanofibers for Optoelectronic Devices. *J. Mater. Chem. C* **2014**, *2*, 5730−5746.

(9) Agbolaghi, S.; Zenoozi, S. A Comprehensive Review on Poly(3-alkylthiophene)-Based Crystalline Structures, Protocols and Electronic Applications. *Org. Electron.* **2017**, *51*, 362−403.

(10) Roy, I.; Hazra, S. Poor Solvent and Thermal Annealing Induced Ordered Crystallites in Poly(3-dodecylthiophene) Films. *RSC Adv.* **2015**, *5*, 665−675.

(11) Tremel, K.; Ludwigs, S. In *P3HT Revisited-From Molecular Scale to Solar Cell Devices*; Ludwigs, S., Ed.; Springer: Berlin, Germany, 2014; pp 39−82.

(12) Roy, I.; Hazra, S. Solvent Dependent Ordering of Poly(3-dodecylthiophene) in Thin Films. *Soft Matter* **2015**, *11*, 3724−3732.

(13) Sirringhaus, H.; Brown, P. J.; Friend, R. H.; Nielsen, M. M.; Bechgaard, K.; Langeveld-Voss, B. M. W.; Spiering, A. J. H.; Janssen, R. A. J.; Meijer, E. W.; Herwig, P.; de Leeuw, D. M. Two-Dimensional Charge Transport in Self-Organized, High-Mobility Conjugated Polymers. *Nature* **1999**, *401*, 685−688.

(14) Jimison, L. H.; Toney, M. F.; McCulloch, I.; Heeney, M.; Salleo, A. Charge-Transport Anisotropy due to Grain Boundaries in Directionally Crystallized Thin Films of Regioregular Poly(3-hexylthiophene). *Adv. Mater.* **2009**, *21*, 1568−1572.

(15) Pandey, M.; Kumari, N.; Nagamatsu, S.; Pandey, S. S. Recent Advances in the Orientation of Conjugated Polymers for Organic Field-Effect Transistors. *J. Mater. Chem. C* **2019**, *7*, 13323−13351.

(16) Gargi, D.; Kline, R. J.; DeLongchamp, D. M.; Fischer, D. A.; Toney, M. F.; O'Connor, B. T. Charge Transport in Highly Face-on Poly(3-hexylthiophene) Films. *J. Phys. Chem. C* **2013**, *117*, 17421−17428.

(17) Kline, R. J.; McGehee, M. D. Morphology and Charge Transport in Conjugated Polymers. *J. Macromolecular Sci., Part C: Polym. Rev.* **2006**, *46*, 27−45.

(18) Sauvé, G.; Javier, A. E.; Zhang, R.; Liu, J.; Sydlik, S. A.; Kowalewski, T.; McCullough, R. D. Well-defined, High Molecular Weight Poly(3-alkylthiophene)s in Thin-Film Transistors: Side Chain Invariance in Field-Effect Mobility. *J. Mater. Chem.* **2010**, *20*, 3195−3201.

(19) Bao, Z.; Feng, Y.; Dodabalapur, A.; Raju, V. R.; Lovinger, A. J. High-Performance Plastic Transistors Fabricated by Printing Techniques. *Chem. Mater.* **1997**, *9*, 1299−1301.

(20) Kline, R. J.; McGehee, M. D.; Kadnikova, E. N.; Liu, J.; Fréchet, J. M. J. Controlling the Field-Effect Mobility of Regioregular Polythiophene by Changing the Molecular Weight. *Adv. Mater.* **2003**, *15*, 1519−1522.

(21) Park, Y. D.; Kim, D. H.; Jang, Y.; Cho, J. H.; Hwang, M.; Lee, H. S.; Lim, J. A.; Cho, K. Effect of Side Chain Length on Molecular Ordering and Field-Effect Mobility in Poly(3-alkylthiophene) Transistors. *Org. Electron.* **2006**, *7*, 514−520.

(22) Salammal, S. T.; Mikayelyan, E.; Grigorian, S.; Pietsch, U.; Koenen, N.; Scherf, U.; Kayunkid, N.; Brinkmann, M. Impact of Thermal Annealing on the Semicrystalline Nanomorphology of Spin-Coated Thin Films of Regioregular Poly(3-alkylthiophene)s as Observed by High-Resolution Transmission Electron Microscopy and Grazing Incidence X-ray Diffraction. *Macromolecules* **2012**, *45*, 5575−5585.

(23) Chang, J.-F.; Sun, B.; Breiby, D. W.; Nielsen, M. M.; Sölling, T. I.; Giles, M.; McCulloch, I.; Sirringhaus, H. Enhanced Mobility of Poly(3-hexylthiophene) Transistors by Spin-coating from High-Boiling-Point Solvents. *Chem. Mater.* **2004**, *16*, 4772−4776.

(24) Saifuddin, M.; Mukhopadhyay, M.; Biswas, A.; Gigli, L.; Plaisier, J. R.; Hazra, S. Tuning the Edge-on Oriented Ordering of Solution-Aged Poly(3-hexylthiophene) Thin Films. *J. Mater. Chem. C* **2020**, *8*, 8804−8813.
(25) Joseph Kline, R.; McGehee, M. D.; Toney, M. F. Highly Oriented Crystals at the Buried Interface in Polythiophene Thin-Film Transistors. *Nat. Mater.* **2006**, *5*, 222−228.
(26) Brinkmann, M.; Wittmann, J. C. Orientation of Regioregular Poly(3-hexylthiophene) by Directional Solidification: A Simple Method to Reveal the Semicrystalline Structure of a Conjugated Polymer. *Adv. Mater.* **2006**, *18*, 860−863.
(27) Verploegen, E.; Miller, C. E.; Schmidt, K.; Bao, Z.; Toney, M. F. Manipulating the Morphology of P3HT-PCBM Bulk Heterojunction Blends with Solvent Vapor Annealing. *Chem. Mater.* **2012**, *24*, 3923−3931.
(28) Chang, J.-F.; Clark, J.; Zhao, N.; Sirringhaus, H.; Breiby, D. W.; Andreasen, J. W.; Nielsen, M. M.; Giles, M.; Heeney, M.; McCulloch, I. Molecular-Weight Dependence of Interchain Polaron Delocalization and Exciton Bandwidth in High-Mobility Conjugated Polymers. *Phys. Rev. B* **2006**, *74*, 115318.
(29) Clark, J.; Chang, J.-F.; Spano, F. C.; Friend, R. H.; Silva, C. Determining Exciton Bandwidth and Film Microstructure in Polythiophene Films Using Linear Absorption Spectroscopy. *Appl. Phys. Lett.* **2009**, *94*, 117.
(30) Don Park, Y.; Lim, J. A.; Lee, H. S.; Cho, K. Interface Engineering in Organic Transistors. *Mater. Today* **2007**, *10*, 46−54.
(31) Dong, H.; Jiang, L.; Hu, W. Interface Engineering for High-Performance Organic Field-Effect Transistors. *Phys. Chem. Chem. Phys.* **2012**, *14*, 14165−14180.
(32) Spano, F. C.; Silva, C. H-and J-aggregate Behavior in Polymeric Semiconductors. *Annu. Rev. Phys. Chem.* **2014**, *65*, 477−500.
(33) Yan, M.; Rothberg, L. J.; Kwock, E. W.; Miller, T. M. Interchain Excitations in Conjugated Polymers. *Phys. Rev. Lett.* **1995**, *75*, 1992−1995.
(34) Parratt, L. J. Surface Studies of Solids by Total Reflection of X-rays. *Phys. Rev.* **1954**, *95*, 359−369.
(35) Tolan, M. *X-ray Scattering from Soft-Matter Thin Films: Materials Science and Basic Science;* Springer: Berlin, Germany, 1999.
(36) Bal, J. K.; Hazra, S. Interfacial Role in Room-Temperature Diffusion of Au into Si Substrates. *Phys. Rev. B* **2007**, *75*, 205411.
(37) Chatterjee, P.; Hazra, S.; Amenitsch, H. Substrate and Drying Effect in Shape and Ordering of Micelles Inside CTAB−Silica Mesostructured Films. *Soft Matter* **2012**, *8*, 2956−2964.
(38) Bal, J. K.; Hazra, S. Time-Evolution Growth of Ag Nanolayers on Differently-Passivated Si(001) Surfaces. *Phys. Rev. B* **2009**, *79*, 155412.
(39) Chatterjee, P.; Hazra, S. Time Evolution of a Cl-Terminated Si Surface at Ambient Conditions. *J. Phys. Chem. C* **2014**, *118*, 11350−11356.
(40) Mukhopadhyay, M.; Hazra, S. Interfacial and Thermal Energy Driven Growth and Evolution of Langmuir−Schaefer Monolayers of Au-Nanoparticles. *Phys. Chem. Chem. Phys.* **2018**, *20*, 1051−1062.
(41) Giri, R. P.; Chakrabarti, A.; Mukhopadhyay, M. K. Cholesterol-Induced Structural Changes in Saturated Phospholipid Model Membranes Revealed Through X-ray Scattering Technique. *J. Phys. Chem. B* **2017**, *121*, 4081−4090.
(42) Roy, S.; Saifuddin, M.; Mandal, S.; Hazra, S. Stearic Acid Mediated Growth of Edge-on Oriented Bilayer Poly(3-hexylthiophene) Langmuir Films. *J. Colloid Interface Sci.* **2022**, *606*, 1153−1162.
(43) Sim, M.; Shin, J.; Shim, C.; Kim, M.; Jo, S. B.; Kim, J.-H.; Cho, K. Dependence of Exciton Diffusion Length on Crystalline Order in Conjugated Polymers. *J. Phys. Chem. C* **2014**, *118*, 760−766.
(44) Yamagata, H.; Spano, F. C. Interplay Between Intrachain and Interchain Interactions in Semiconducting Polymer Assemblies: The HJ-aggregate Model. *J. Chem. Phys.* **2012**, *136*, 184901.
(45) Spano, F. C. Modeling Disorder in Polymer Aggregates: The Optical Spectroscopy of Regioregular Poly(3-hexylthiophene) Thin Films. *J. Chem. Phys.* **2005**, *122*, 234701.
(46) Clark, J.; Silva, C.; Friend, R. H.; Spano, F. C. Role of Intermolecular Coupling in the Photophysics of Disordered Organic Semiconductors: Aggregate Emission in Regioregular Polythiophene. *Phys. Rev. Lett.* **2007**, *98*, 206406.
(47) Nagarjuna, G.; Baghgar, M.; Labastide, J. A.; Algaier, D. D.; Barnes, M. D.; Venkataraman, D. Tuning Aggregation of Poly(3-hexylthiophene) Within Nanoparticles. *ACS Nano* **2012**, *6*, 10750−10758.
(48) Kleinhenz, N.; Persson, N.; Xue, Z.; Chu, P. H.; Wang, G.; Yuan, Z.; McBride, M. A.; Choi, D.; Grover, M. A.; Reichmanis, E. Ordering of Poly(3-hexylthiophene) in Solutions and Films: Effects of Fiber Length and Grain Boundaries on Anisotropy and Mobility. *Chem. Mater.* **2016**, *28*, 3905−3913.
(49) Manas, E. S.; Spano, F. C. Absorption and Spontaneous Emission in Aggregates of Conjugated Polymers. *J. Chem. Phys.* **1998**, *109*, 8087−8101.
(50) Roehling, J. D.; Arslan, I.; Moule, A. J. Controlling Microstructure in Poly(3-hexylthiophene) Nanofibers. *J. Mater. Chem.* **2012**, *22*, 2498−2506.
(51) Causin, V.; Marega, C.; Marigo, A.; Valentini, L.; Kenny, J. M. Crystallization and Melting Behavior of Poly(3-butylthiophene), Poly(3-octylthiophene), and Poly(3-dodecylthiophene). *Macromolecules* **2005**, *38*, 409−415.
(52) Kiessig, H. Interferenz von Röntgenstrahlen an dünnen Schichten. *Ann. Phys.* **1931**, *402*, 769−788.
(53) Gibaud, A.; Hazra, S. X-ray Reflectivity and Diffuse Scattering. *Curr. Sci.* **2000**, *78*, 1467−1477.
(54) Gibaud, A.; Vignaud, G. In *X-ray and Neutron Reflectivity: Principles and Applications;* Daillant, J., Gibaud, A., Eds.; Springer: Berlin, Germany, 2009; pp 85−131.
(55) Roy, I.; Hazra, S. Structures of Spin-Coated and Annealed Monolayer and Multilayer Poly(3-dodecylthiophene) Thin Films. *RSC Adv.* **2017**, *7*, 2563−2572.
(56) Qu, Y.; Su, Q.; Li, S.; Lu, G.; Zhou, X.; Zhang, J.; Chen, Z.; Yang, X. H-Aggregated Form II Spherulite of Poly(3-butylthiophene) Grown from Solution. *ACS Macro Lett.* **2012**, *1*, 1274−1278.
(57) Hlaing, H.; Lu, X.; Hofmann, T.; Yager, K.; Black, C.; Ocko, B. Nanoimprint-Induced Molecular Orientation in Semiconducting Polymer Nanostructures. *ACS Nano* **2011**, *5*, 7532−7538.


https://doi.org/10.1021/acsapm.1c01772
*ACS Appl. Polym. Mater.* 2022, 4, 1377−1386